

UKAEA-CCFE-PR(19)18

D A Ryan, M Dunne, A Kirk, S Saarelma, W Suttrop,  
C Ham, Y Q Liu, M Willensdorfer, the ASDEX  
Upgrade team, the MST1 team

# **Numerical survey of predicted peeling response in ELM mitigated and suppressed phases on ASDEX Upgrade**

Enquiries about copyright and reproduction should in the first instance be addressed to the UKAEA Publications Officer, Culham Science Centre, Building K1/O/83 Abingdon, Oxfordshire, OX14 3DB, UK. The United Kingdom Atomic Energy Authority is the copyright holder.

The contents of this document and all other UKAEA Preprints, Reports and Conference Papers are available to view online free at [scientific-publications.ukaea.uk/](https://scientific-publications.ukaea.uk/)

# **Numerical survey of predicted peeling response in ELM mitigated and suppressed phases on ASDEX Upgrade**

D A Ryan, M Dunne, A Kirk, S Saarelma, W Suttrop, C Ham, Y Q Liu, M Willensdorfer, the ASDEX Upgrade team, the MST1 team



# Numerical survey of predicted peeling response in ELM mitigated and suppressed phases on ASDEX Upgrade

D A Ryan<sup>1</sup>, M Dunne<sup>2</sup>, A Kirk<sup>1</sup>, S Saarelma<sup>1</sup>, W Suttrop<sup>2</sup>, C Ham<sup>1</sup>, Y Q Liu<sup>3</sup>, M Willensdorfer<sup>2</sup>, the ASDEX Upgrade team<sup>2</sup> and the MST1 team[1]

<sup>1</sup> CCFE, Culham Science Centre, Abingdon, Oxfordshire, UK

<sup>2</sup> Max Planck Institute for Plasma Physics, Garching, Germany

<sup>3</sup> General Atomics, P. O. Box 85608, San Diego, California 92186-5608, USA

**Abstract.** Using the MARS-F linear MHD code (Liu *et al* 2000 *Phys. Plasmas* **7** 3681), a numerical survey of the plasma response to applied RMPs in ASDEX Upgrade ELM control experiments is conducted, to clarify the role of triangularity and the peeling response in the suppression mechanism. The peeling response is found to decrease with increasing triangularity, due to an increase in the coil-plasma gap reducing the effective vacuum field. Therefore the hypothesis that the requirement of high triangularity for suppression access is due to the requirement of a sufficiently large peeling response[2] is suspected to be incorrect. A secondary hypothesis is proposed, that in high triangularity the drive of the resonant response by the peeling response may be boosted by enhanced poloidal harmonic coupling, which could explain the requirement of high triangularity for suppression access. It is shown that in fact the poloidal harmonic coupling between the resonant and off-resonant components decreases with triangularity, and therefore this hypothesis is also rejected. Finally an alternative hypothesis is discussed, that high triangularity is required to access suppression because the associated enhanced pedestal stability allows the edge deformation to be large enough to control the density, without the reduction in stability due to boundary deformation destabilising ELMs. Results here are consistent with this hypothesis, however a rigorous test requires models to be developed to compute the stability of experimental 3D equilibria.

## 1. Introduction

The ITER tokamak is expected to operate primarily in an ELM-y H-mode regime, which features a quasi-periodic MHD instability known as the Edge Localised Mode (ELM). ELMs are triggered when the edge pedestal exceeds a stability threshold in pressure gradient or current[3]. The ensuing collapse in the pedestal pressure causes a short transient of high heat flux to impact the plasma facing components, which is expected to exceed the material damage limit of the ITER divertor if left unmitigated[4]. However, it has been demonstrated that the application of Resonant Magnetic Perturbations (RMPs) may prevent ELMs from being triggered, while retaining stable H-mode operation, a regime referred to as ELM suppression[5]. The suppressed regime is accessible only in certain small regions of parameter space[6], and the access conditions are not known comprehensively. ELM mitigation is a more readily accessible regime[6], in which the RMPs cause the ELMs to trigger at a faster rate, which reduces the energy content and peak heat flux of individual ELMs[7]. Applying non-axisymmetric RMPs to a 2D plasma equilibrium causes 3D deformation of the plasma flux surfaces, colloquially known as corrugation[8, 9]. The resulting 3D equilibrium has reduced P-B stability relative to the unperturbed 2D equilibrium, which is suspected to be the driving mechanism for ELM mitigation[10, 11, 12, 13]. The ITER design includes a flexible set of RMP coils[14], and ELM suppression has now been reproduced on many major tokamaks currently operating[5, 15, 16, 17]. Intensive research efforts are focused on developing a robust and predictive theory of ELM suppression, which may be used to assess the capability of ITER to reliably suppress ELMs. It is widely accepted that any theory of ELM suppression or mitigation must properly account for the plasma response to the applied RMPs [18, 19, 20]. The components of the applied field aligned to the equilibrium magnetic field, commonly referred to as the resonant field or pitch aligned field, must be finite for magnetic islands to form in the plasma. The plasma response typically manifests as a strong screening of the resonant field, and also the amplification of marginally stable MHD modes in the plasma bulk, a process referred to as Resonant Field Amplification. A particular class of these stable modes are of interest here, localised to the plasma edge with poloidal mode numbers just above resonance, commonly referred to as the peeling response[21]. It is predicted theoretically that the amplified peeling response may drive the resonant field via poloidal harmonic coupling[21], and the corrugation induced by the peeling response is also observed to correlate with RMP induced density pump out[22]. It is commonly observed experimentally[15, 17, 19] that ELM suppression is achieved when the applied field is tuned to maximise the peeling response, which may be due to the role of the peeling response in driving the resonant field, or in controlling the density via density pump out. The peeling response also correlates with the mitigated ELM frequency, possibly due to the deleterious effect of increasing edge corrugation on P-B stability. It seems that the peeling response may have a crucial role in determining both the transport and stability properties of RMP perturbed plasmas, which must be further clarified.

Recent experimental campaigns on ASDEX Upgrade have achieved complete ELM

suppression, demonstrating that tuning the applied field to optimally amplify the peeling response, and achieving a sufficiently high upper triangularity  $\delta_U$ , are crucial suppression access parameters. It is proposed in [2], that increasing  $\delta_U$  allows access to higher pedestal pressures, which boosts the peeling response and thereby facilitates suppression access. In this work, the role of  $\delta_U$  and the peeling response in achieving ELM suppression is investigated using a numerical survey of the plasma response in experimental conditions. It is found that in experiments, increasing  $\delta_U$  moves the plasma boundary away from the RMP coils, reducing the effective vacuum field and consequently the peeling response. This effect dominates over the modest increase in peeling response due to increased pedestal pressure, resulting in a net decrease of the peeling response with triangularity. This implies that the hypothesis described previously for explaining the high  $\delta_U$  requirement [2], is likely to be incorrect.

An alternative hypothesis is proposed, that the requirement of high triangularity may be a consequence of increased triangularity induced  $\Delta m = 3$  poloidal harmonic coupling (PHC). Increasing  $\Delta m = 3$  PHC may allow the peeling response to drive the resonant field more efficiently, increasing the resonant field for fixed peeling response. This suggestion is tested with a numerical scan of the upper triangularity, and with the survey. It is found that while triangularity induced PHC coupling does increase with  $\delta_U$  as expected, it is more than compensated by a decrease in toroidicity induced  $\Delta m = 1$  coupling. The result is that the drive of the resonant components by PHC is found to decrease with  $\delta_U$ , so this explanation for the high triangularity requirement for suppression is rejected.

Finally, an alternative explanation of the requirement for high triangularity is described, to be tested in future works. Following [10], it is explained that edge corrugation driven by the peeling response degrades P-B stability. Movement of the P-B stability boundary may compensate for movement of the operational point towards the stable region as the peeling response and density pump out increase, keeping the operational point P-B unstable. In principle, the enhanced P-B stability of high triangularity plasmas would increase their resilience to corrugation induced destabilisation, which may explain the requirement of high triangularity for suppression access.

In section 2, the database of ASDEX Upgrade ELM control experiments is described, metrics used to characterise the plasma response are explained and compared, and pedestal properties which may affect the peeling response are examined. In section 3, the plasma response to experimentally applied RMP fields is computed using the MARS-F linear MHD code, using the database points as model input, and the dependence of the peeling response on  $\delta_U$  and pedestal pressure examined. In section 4 the proposal that the high triangularity requirement for suppression may be related to enhanced triangularity induced poloidal harmonic coupling, is investigated using a numerical scan of the upper triangularity and the equilibrium database. In section 5 the results are discussed, and a testable hypothesis for the  $\delta_U$  requirement outlined.

## 2. ASDEX Upgrade ELM Control Database

Numerous RMP ELM control campaigns on ASDEX Upgrade have recently been conducted, adding many examples of both mitigation and suppression[2, 23] to the experimental archive. In this section, the assembled database of points from selected ASDEX Upgrade ELM control experiments is described. Points are chosen from both high and low  $\delta_U$  RMP ELM control experiments in which either suppression or mitigation was achieved, avoiding close temporal proximity to transitions into or out of suppression. For mitigated phases, the ELM frequency at each point is extracted and included in the database. Quantifying the extent of mitigation relative to the natural ELM frequency is beyond the scope of this study, so for simplicity this work will define 'good' mitigation as  $f_{ELM} > 200$ , and 'poor' mitigation as  $f_{ELM} < 200$ . For each chosen point, an mtanh function[24] is fitted to experimental measurements of  $T_e$ ,  $T_i$ ,  $n_e$ , and a spline to toroidal bulk rotation velocity  $v_T$ , with a 20ms integration time. When appropriate, a radial shift is applied to the  $T_e$  data measured using the edge Thompson scattering diagnostic, to enforce  $T_e \approx 100eV$  at the separatrix. To ensure consistency between the  $T_e$  and  $n_e$  profiles, this same shift was then applied to the density profile as measured using the same diagnostic, as performed in [25]. The high frequency of the mitigated ELMs made ELM synchronisation infeasible, however their corresponding small size reduced the effect of individual ELMs on the measured profiles such that ELM synchronisation was deemed unnecessary. An equilibrium reconstruction is then manually performed for each point using the CLISTE[26] equilibrium code, constrained by magnetic measurements integrated over the same period as the kinetic profiles, and using the measured kinetic profiles to constrain the edge pressure profile. The experimentally applied RMP coil currents are extracted from the experimental archive, and corrections for the field attenuation due to eddy currents in the passive stability loops (PSLs) are computed using a finite element modelling code[27] as in previous studies[28], and applied as scaling factors in post processing. Using this data as model input, the plasma response to the applied field is then computed using the extensively benchmarked and validated [29, 30, 31] linear MHD code MARS-F [32], and the peeling response quantified using metrics described below. The database points are clustered around  $(R_0, B_0, I_p) = (1.70m, 1.75T, 0.80MA)$  with wide spread. So that the effect of varying  $\delta_U$  may be examined, points were taken from low and high  $\delta_U$  experiments.

### 2.1. Peeling response scalar metrics

In previous studies it has been shown that ELM control observations are strongly correlated with certain metrics derived from the plasma response, the most widely used of which are the outermost resonant component of the total magnetic perturbation  $|b_{res}^1|$  (correlated with ELM frequency[13]), and the normal displacement of the plasma surface around the X point  $|\xi_n X(s=1)|$  (correlated with density pump out[22]). These metrics are suitable for studies of a single plasma equilibrium, or for coil optimisation studies for which they have been used in the past[28, 33]. In these studies, the dependence of the metrics on the coil phase

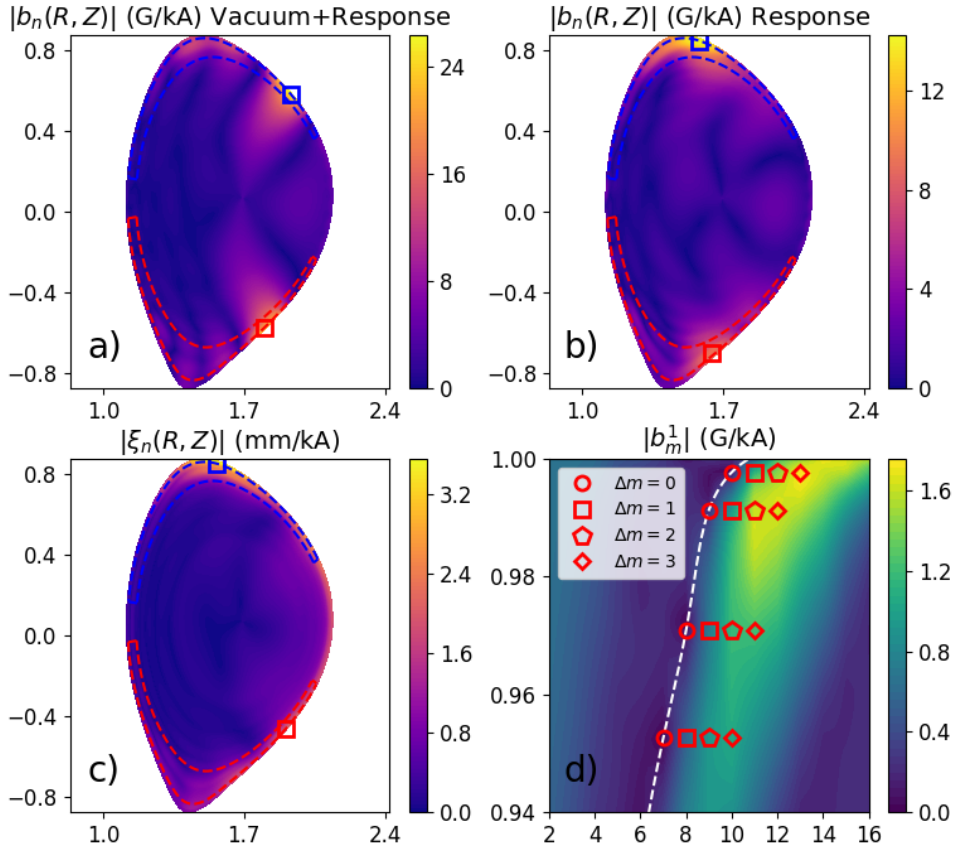


**Figure 1.** Explanations of the metrics used here to quantify the plasma response. a)  $b_n T_{tot}$  and  $b_n X_{tot}$  are the total magnetic perturbation (sum of vacuum field and plasma response) maximised over the regions outlined above, near the plasma top and plasma X point. The squares denote the location of maximal total field for this example, where  $b_n T_{tot}$  and  $b_n X_{tot}$  are measured. b)  $b_n T_{resp}$  and  $b_n X_{resp}$  are the magnetic plasma response (total - vacuum) maximised over the same regions. c)  $\xi_n T$  and  $\xi_n X$  are the plasma displacement normal to flux surfaces, maximised over the same regions. d) Spectral magnetic metrics  $b_{m=nq+\Delta m}^1$  refer to the outermost off resonant components of the total magnetic perturbation, normal to flux surfaces.

difference was the crucial quantity, which is robust to the degree of boundary distortion required to truncate the X point. However the absolute values of  $|b_{res}^1|$  and  $|\xi_n X(s=1)|$  as previously used are not strictly robust to X point truncation, and so are unsuitable for comparison between different equilibria which this study is concerned with. In this work, simplified metrics are chosen to capture the edge peeling plasma response while being robust to truncation. Bulk magnetic metrics  $b_n\{T/X\}\{tot/resp\}$  refer to the total (*tot*) or pure response (*resp*) magnetic field normal to flux surfaces maximised over the plasma top (*T*) or X point (*X*) regions. The regions over which the magnetic field is maximised are sketched in Figure 1. We distinguish between the total magnetic field and pure response (ie, total -

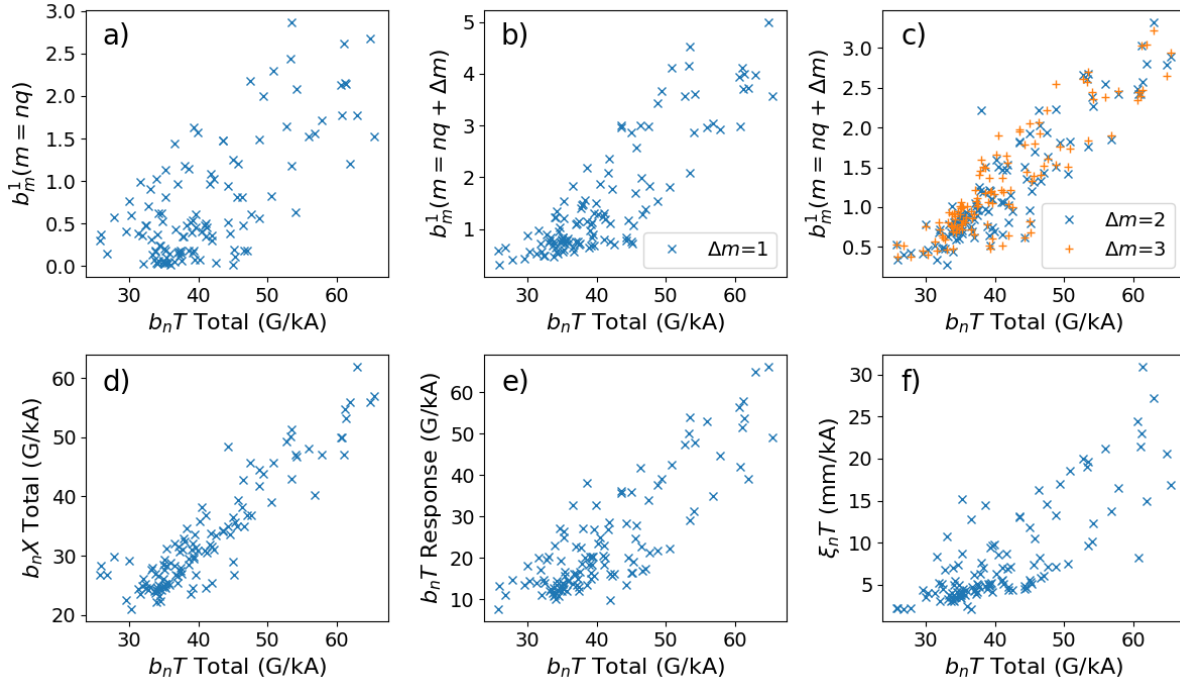


**Figure 2.** For each point in the database, the plasma response to a fixed static 1kA (5kAt) field with a fixed coil phase difference  $\Delta\phi_{ul} = 90$  degrees is computed with MARS-F, and scalar metrics extracted. a) Outermost resonant component plotted against  $b_n T_{tot}$ . b,c) Outermost off resonant components plotted against  $b_n T_{tot}$ . d)  $b_n X_{tot}$  plotted against  $b_n T_{tot}$ . e)  $b_n T_{resp}$  plotted against  $b_n T_{tot}$ . f)  $\xi_n T$  plotted against  $b_n T_{tot}$ .

vacuum field) since the former is indicative of the 'real' field which may be measured in experiments, while the latter more closely corresponds to the peeling response since it does not contain the vacuum field. Since the edge peeling response commonly manifests in the  $(m = nq + 2, 3)$  spectral region, a spectral magnetic metric  $b_{m=nq+\Delta m}^1$  for  $\Delta m = 1, 2, 3$  is used, referring to the outermost 'off-resonant' components of the total magnetic field. Displacement metrics  $\xi_n \{T/X\}$  refer to the plasma displacement normal to flux surfaces, maximised over the plasma top ( $T$ ) or X point ( $X$ ) regions.

For each point in the database, the plasma response to a fixed static 1kA (5kAt) field with a fixed coil phase difference  $\Delta\phi_{ul} = 90$  degrees is computed with MARS-F (in later sections, the experimental coil currents are used and PSL corrections included). It is previously observed that magnetic and displacement metrics and their corresponding experimental observables, have similar dependencies on the coil phase difference  $\Delta\phi_{ul}$  [34, 35, 28]. It is also expected that this set of metrics will be correlated with each other even for fixed  $\Delta\phi_{ul}$  and applied field, and therefore one metric may be used as a proxy for the others. Figure 2 plots the peeling response metrics against the total magnetic perturbation in the plasma top region  $b_n T_{tot}$ , using a constant applied field amplitude of 1kA (5kAt) with a fixed coil phase difference  $\Delta\phi_{ul} = 90$  degrees. Figure 2a) plots  $b_n T_{tot}$  against the outermost resonant component  $b_{m=nq}^1$ . Although the applied field is constant, a correlation is apparent between

the resonant component and  $b_n T_{tot}$ . This is consistent with previous predictions[21] that the resonant field may be driven by the edge peeling response via poloidal harmonic coupling. However, numerical truncation of the plasma X point modifies the edge safety factor profile, causing the location of the outermost resonant component to move relative to the resistivity and rotation profiles. This introduces a potentially large uncertainty into the absolute value of  $b_{m=nq}^1$ , and it is therefore not used as a metric for the peeling response in this study. Figures 2b) and c) plot  $b_n T_{tot}$  against the off-resonant components  $b_{m=nq+\Delta m}^1$  for  $\Delta m = 1, 2, 3$ . The strong correlations apparent suggest that the peeling response may be assessed either using the spectral or bulk metrics. It is also consistent with the common observation that the peeling response manifests primarily in the spectral region of  $m = nq + \Delta m$  for  $\Delta m = 1, 2, 3$ . Figure 2d) plots  $b_n X_{tot}$  against  $b_n T_{tot}$ . The strong correlation indicates that the peeling response may be measured either at the plasma top or bottom without significantly affecting the results. This is useful since we may avoid any possible issues arising from truncation of the plasma X point, by simply choosing the plasma top region to focus on in this study. Figure 2e) plots  $b_n T_{tot}$  against  $b_n T_{resp}$ . Correlation is trivially expected since the total field is the sum of the vacuum field and response, and also because since the plasma response is an amplification of the vacuum field and is therefore proportional to it. However the correlation is somewhat confounded since the two metrics are measured at different locations in the poloidal plane, as demonstrated by Figures 1a,b). In the majority of cases, the total magnetic field at the plasma edge is dominated by the vacuum field, and so the maximum where  $b_n T_{tot}$  is measured is found at the point closest to the coils (for consistency, points where this is not the case are excluded), while the maximum of the plasma response where  $b_n T_{resp}$  is measured tends to be in a region of low  $B_p$ , ie, at the plasma top. Figure 2f) plots  $b_n T_{tot}$  against the maximum displacement in the plasma top region  $\xi_n T$ , demonstrating the correlation between plasma displacement and total field previously observed for scans of coil phase  $\Delta\phi_{ul}$ . The metrics chosen are highly correlated with each other, so the precise choice of whether to characterise the plasma response using the X point or plasma top region, total magnetic field, pure response field or displacement, has limited significance.

## 2.2. Pressure dependence on $\delta_U$

The hypothesis outlined in [2] for the high  $\delta_U$  requirement for suppression proposes that the pedestal pressure increases with  $\delta_U$ , in order to boost the pressure drive for the peeling response. Figure 3 plots the equilibrium pressure at the pressure pedestal and  $s=0.99$ , against upper triangularity  $\delta_U$  for the dataset points. The database also contains points from an experimental scan of  $\delta_U$  in discharge 34835, which is also plotted in the figure. To reduce the input power as a confounding variable, a filter is applied to restrict  $\beta_N$  to within  $1.7 < \beta_N < 2.1$  (the points from the 34835 scan are not subject to this constraint). The plots indicate that the pedestal pressure does increase with  $\delta_U$  as expected, consistent with [25] and validating this part of the original hypothesis.

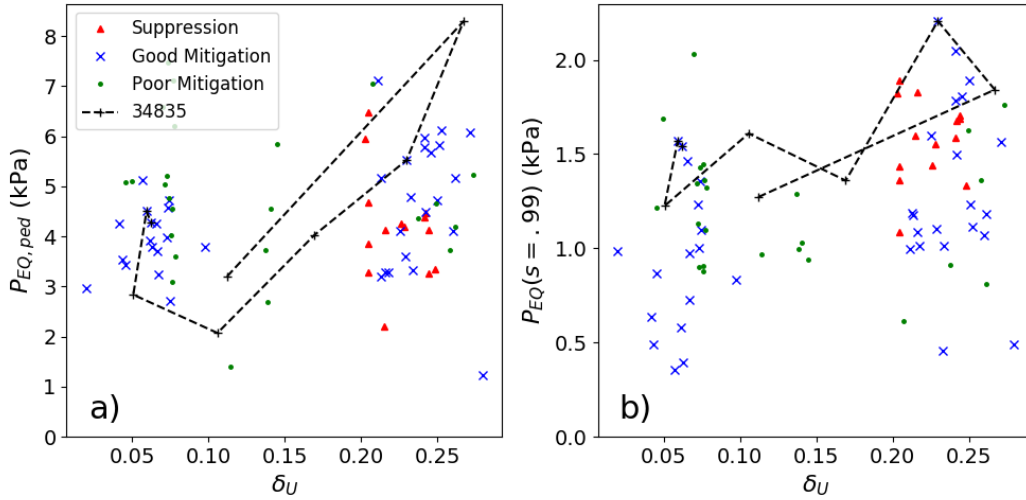


**Figure 3.** a) Equilibrium pedestal pressure against plasma triangularity. b) Equilibrium plasma pressure at the  $s = \sqrt{\psi_N} = 0.99$  surface against plasma triangularity.

### 2.3. Pressure dependence on density

It is established experimentally[15] that suppression access requires the density to be reduced below some critical value. This implies that the pedestal pressure, dominated by the thermal pressure, will be reduced in suppressed relative to mitigated cases. This would imply a lower pressure drive for the peeling response, and may lead to the peeling response being systematically lower in the suppressed cases relative to mitigated. Figure 4a) plots the equilibrium plasma pressure against electron number density at their respective pedestals, for the high triangularity points ( $0.18 < \delta_U < 0.28$ ). It appears that the edge density of the suppression discharges being capped at around  $3 \times 10^{19} m^{-3}$ , does result in the pedestal pressure being systematically lower in suppression than mitigation. Figure b) plots the sum of  $T_i + T_e$  against  $n_e$  at their respective pedestals for the same points (neglecting  $Z_{eff}$ ). The figure indicates that the loss of density in the suppression phase is not compensated by higher particle temperatures, resulting in a lower pedestal pressure. This result leads us to expect slightly reduced pressure drive of the peeling response between the suppressed and mitigated phases for fixed triangularity.

### 3. Peeling response in mitigation and suppression and $\delta_U$ dependence

For each point in the database described previously, the plasma response to the experimentally applied RMP field is computed with MARS-F, and corrected for PSL attenuation. Figure 5a) plots the total bulk magnetic field  $b_n T_{tot}$  against the  $\Delta m = 1$  off resonant component of the total field,  $b_{m=nq+1}^1$ , for cases of mitigation and suppression. Figure 5c) plots the pure magnetic plasma response  $b_n T_{resp}$  against the normal plasma displacement  $\xi_n T$ . The metrics

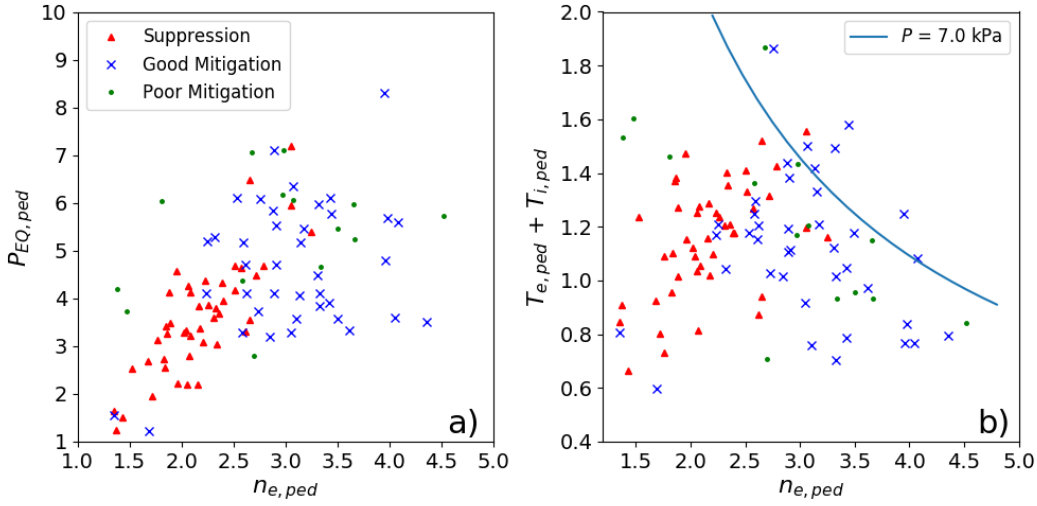
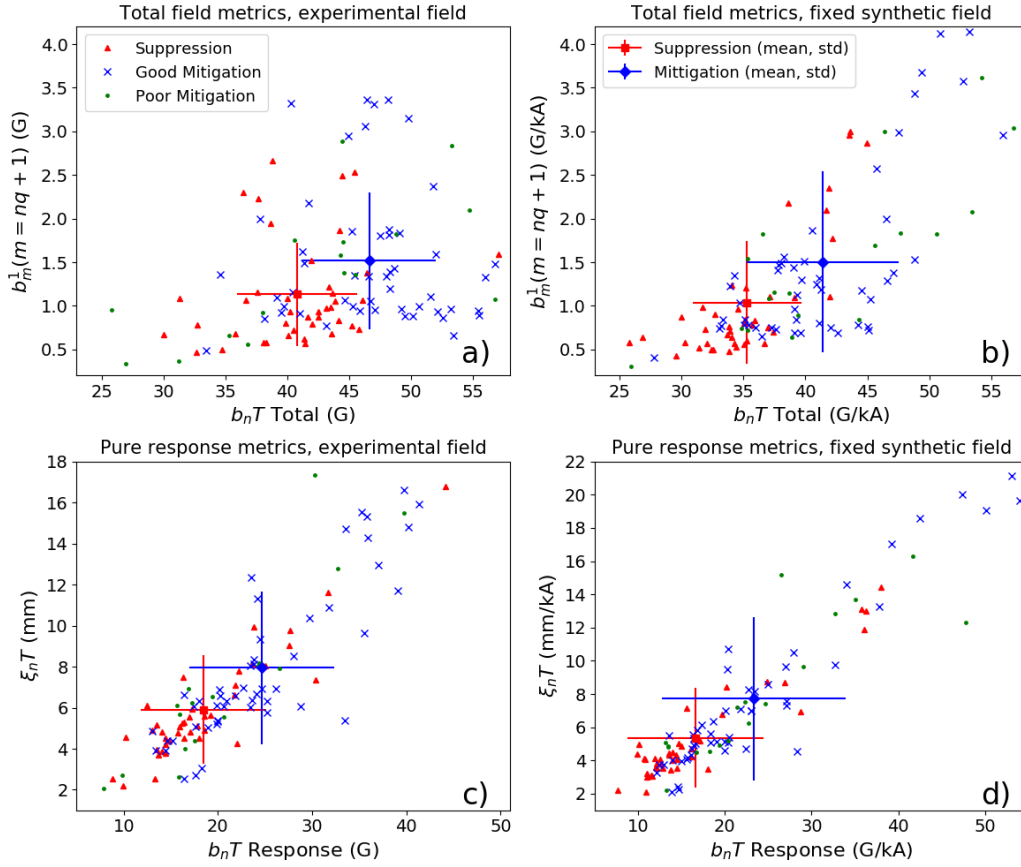


**Figure 4.** a) The thermal plasma pressure (here approximated to simply be  $P_{EQ,ped}$ , plotted against electron number density, both evaluated at their respective pedestals. b) Sum of the ion and electron temperatures plotted against electron number density, evaluated at their respective pedestals.

$b_n T_{tot}$  and  $b_{m=nq+1}^1$  used in figure a) include the vacuum field, meaning that they represent the field which physically exists in experiments and may in principle be measured. However, the vacuum field may confound measurement of the pure plasma response. Metrics  $b_n T_{resp}$  and  $\xi_n T$  used in figure c) are more directly indicative of the plasma response. All model input used to compute the points in figures 5a,c) were derived from experimental machine parameters and experimental measurement. Therefore, we may expect the results plotted in figures a,c) to represent a survey of the peeling response which occurred in the recent ASDEX Upgrade ELM control experimental campaigns. The mean and spread (simple standard deviation) of the mitigation and suppression points separately are also plotted. While the data from the suppression and mitigation sets overlap to a large degree, the averages for each set indicate that, considering the database as a whole, the peeling response tends to be lower in suppression than mitigation. Figures 5b,c) plot these same metrics, but with a fixed applied field of 1kA (5kAt) and coil phase  $\phi_{ul} = 90$ , removing all variation in applied field as in figure 2. The shift to lower peeling response in suppression is still evident in this plot, indicating that it is due to equilibrium variations between the two phases rather than applied field variations.

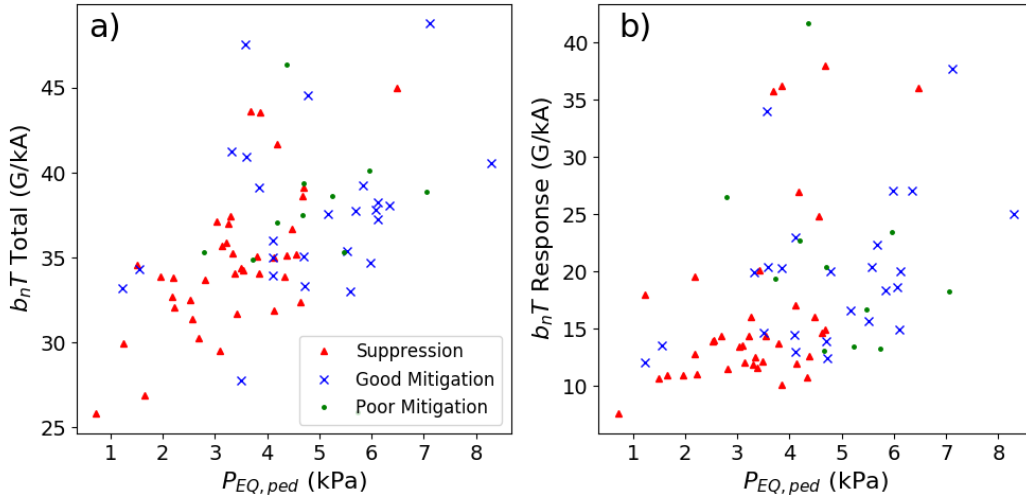
Figures 6a) and b) plot  $b_n T_{tot}$  and  $b_n T_{resp}$  against the equilibrium pedestal pressure for fixed applied field, and with triangularity restricted to  $0.18 < \delta_U < 0.28$ . The plots seem to indicate a small dependence of the peeling response on the pedestal pressure, consistent with the original hypothesis of the high triangularity requirement[2]. Having established a correlation between the triangularity and pressure in figure 3, and between the pressure and peeling response in figure 6 (although it is slight), we may then expect to find a correlation between the triangularity and peeling response.

Figure 7a) plots the peeling response metric  $b_n T_{tot}$  against upper triangularity  $\delta_U$ . The



**Figure 5.** a) Space of plasma response metrics  $b_n T_{tot}$  and  $b_m^1$ , using experimental coil amplitude and phase, and including PSL corrections. This result represents the peeling response which occurred in experiment. b) Space of plasma response metrics  $b_n T_{tot}$  and  $b_m^1$ , using fixed coil amplitude of 5kAt and 90 degree phase, to remove applied field variation as a variable. c) Space of plasma response metrics  $b_n T_{resp}$  and  $\xi_n T$ , using experimental coil amplitude and phase, and including PSL corrections. d) Space of plasma response metrics  $b_n T_{resp}$  and  $\xi_n T$ , using fixed coil amplitude of 5kAt and 90 degree phase.

figure shows that contrary to initial expectations, the total field including peeling response decreases strongly with  $\delta_U$ . The immediate cause of this is demonstrated in figure 7c), which plots the vacuum field at the same location in the poloidal plane the  $b_n T_{tot}$  metric is measured. The figure shows that the vacuum field at the plasma top also decreases with  $\delta_U$ , which causes  $b_n T_{tot}$  to be reduced accordingly. Figure 7b) plots the pure response field  $b_n T_{resp}$  against  $\delta_U$ . Since the response is the amplification of the vacuum field, reduction of the vacuum field with  $\delta_U$  results in a reduction of the plasma response, which is only partially compensated by the increasing pressure drive with increasing  $\delta_U$ . Figure 7d) plots the closest distance between the upper coils and plasma boundary, against triangularity. The field applied at the coils is fixed in this plot, but the effective field which reaches the plasma strongly decreases as the gap between the coils and plasma widens, as shown in figure 7e). It appears that in practice, increasing  $\delta_U$  deforms the plasma away from the coils, such that the vacuum field reaching the plasma, and consequent plasma response, are reduced. This consequence of increasing  $\delta_U$  is



**Figure 6.** Plasma response metrics  $b_n T_{tot}$  and  $b_n T_{resp}$  with fixed applied field, against the pedestal pressure. Triangularity is restricted to  $0.18 < \delta_U < 0.28$ .

demonstrated in figure 8, which plots a high and low  $\delta_U$  plasma boundary, and the gap between the upper and lower coils and plasma computed for the database. It is interesting to note that the effect is not confined to the upper plasma region; the gap between the plasma lower coils also increases with  $\delta_U$ . This effect dominates over the modest boost to the peeling response caused by increased pedestal pressure at high triangularity. Furthermore, referring to only the high  $\delta_U$  points in figures 7a,b), it appears that for fixed triangularity the peeling response is lower in suppression than mitigation. The enhanced density pump out in suppression leading to reduced pressure drive is the probable cause of this.

#### 4. Effect of triangularity on poloidal harmonic coupling mechanism

It has previously been predicted that the resonant component of the total field may be driven by the peeling response via poloidal harmonic coupling (PHC)[21]. PHC is a purely geometric effect, so it is expected to be modified by plasma shaping. In particular, coupling between modes  $m \pm 1$ ,  $m \pm 2$  and  $m \pm 3$  are linked with toroidicity, elongation and triangularity respectively. The amplified peeling response typically manifests in the spectral region just above resonance with  $\Delta m = 2 - 3$ , where  $nq = m + \Delta m$ . It is therefore proposed here that increasing the triangularity may cause an increase in coupling between the resonant field and peeling response. This could contribute to the suppression mechanism by facilitating field penetration and island formation. In this section, a scan of the plasma upper triangularity is performed, to investigate the effect of triangularity on PHC between the peeling response and the resonant field. To eliminate confounding variables, in this section only the vacuum field is considered.

A reference shape is taken from a reconstruction of discharge 30835 at 3.2s, and the

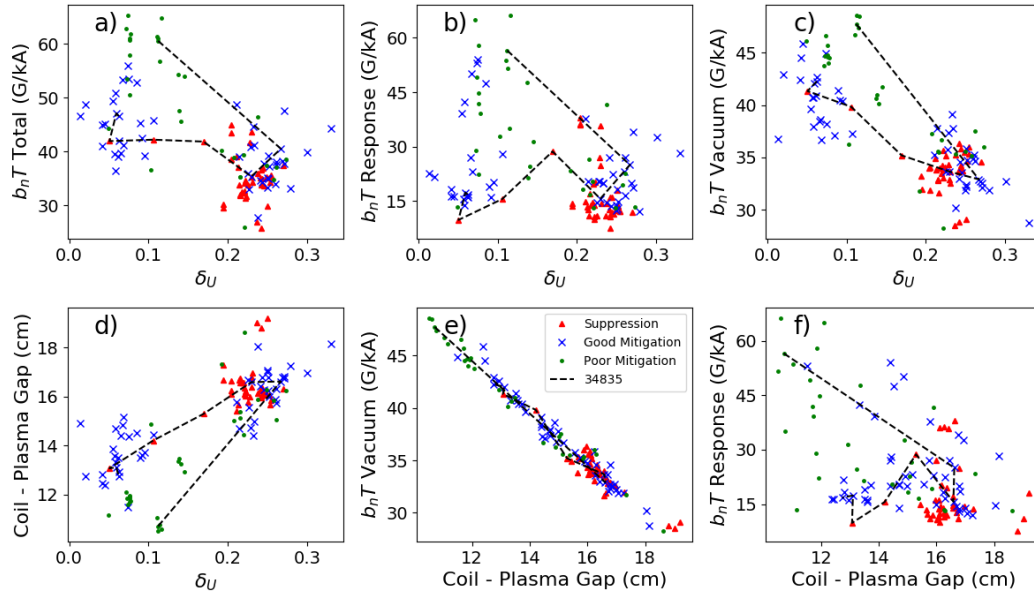


**Figure 7.** a) Total field metric  $b_n T_{tot}$  with fixed applied field, against  $\delta_U$ . b) Pure response metric  $b_n T_{resp}$  against  $\delta_U$ . c) Vacuum field at the same location as  $b_n T_{tot}$  is measured, against triangularity. d) The minimum distance from the upper coils to the plasma edge against  $\delta_U$ . e) The vacuum field at the same location as the metric  $b_n T_{tot}$  is measured, against minimum distance from the coils to the plasma edge. f) Displacement at the plasma top region  $\xi_T$  against the minimum distance from the upper coils to the plasma edge.

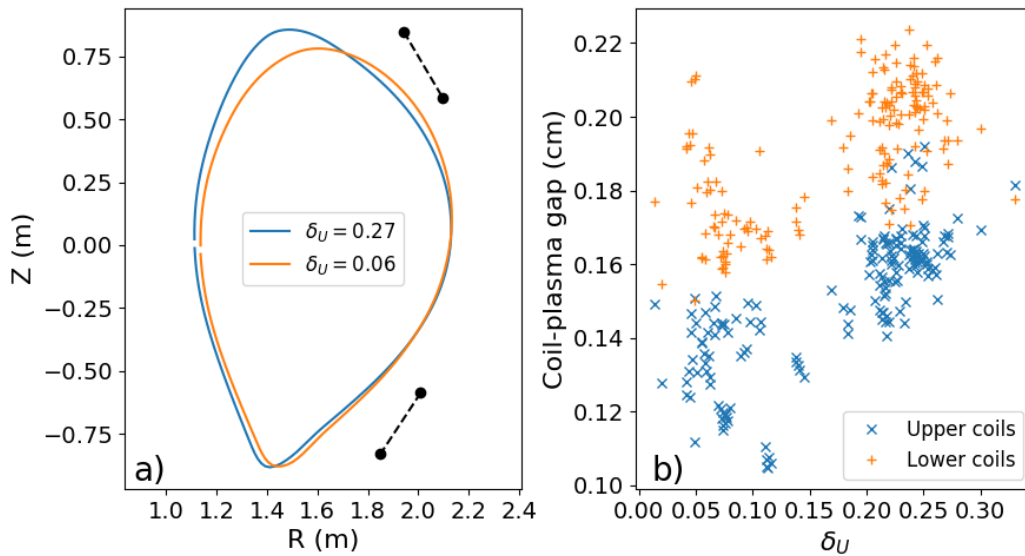


**Figure 8.** a) Plasma boundaries for a high and low  $\delta_U$  plasma, from discharge 34835 at 2.5s and 5.6s respectively. b) Minimum gap between the upper and lower coils (coil location in  $(R,Z)$  taken to be the centre of the window coils) and the plasma boundary.

upper half of the boundary is distorted to scan the upper triangularity. The resulting plasma boundaries are plotted in figure 9a). A vacuum perturbation containing only a single poloidal harmonic  $m_{BC}$  was applied as a boundary condition at the plasma edge, as demonstrated for the highest and lowest triangularity cases in figures 9b) and 9c) respectively. The results in figures 9 and 10 use  $m_{BC} = 12$ , but the results were also found to be general for  $m_{BC} = 10 - 16$ . Figure 10 plots the amplitude of poloidal harmonics of  $b_m^1$  at  $s = 0.997$  with poloidal harmonic numbers  $m_{BC} - 1$ ,  $m_{BC} - 2$  and  $m_{BC} - 3$ , normalised to the  $m_{BC}$  harmonic. The flux surface  $s = 0.997$  was deliberately chosen to be very close to the plasma boundary in order to demonstrate direct  $\Delta m = 1, 2, 3$  coupling with only the  $m_{BC}$  component, and reduce 'secondary' coupling between the  $m = m_{BC} - 1$  and  $m = m_{BC} - 2$  components. The figure shows that while the  $m = m_{BC} - 1$  harmonic decreases relative to  $m_{BC}$ , the harmonics  $m = m_{BC} - 2$  and  $m = m_{BC} - 3$  increase with  $\delta_U$ . This shows that increasing the triangularity may in principle lead to increased  $\Delta m = 2, 3$  coupling between the peeling response and resonant components as proposed, but at a cost of decreased  $\Delta m = 1$  coupling. The figure also shows that the  $m = m_{BC} - 2$  and  $m = m_{BC} - 3$  components are very small relative to the  $m = m_{BC} - 1$  component (note that the  $m = m_{BC} - 2$  and  $m = m_{BC} - 3$  components are rescaled in the figure), indicating that toroidicity induced  $\Delta m = 1$  coupling is far stronger than the triangularity and elongation induced  $\Delta m = 2, 3$  coupling.

Using the previously assembled database and fixed realistic 1kA applied RMP field, we may test whether this finding is robust to realistic fields and varying experimental boundary shapes. Figure 11a) plots  $b_{m=nq}^1/b_{m=nq+1}^1$  (the ratio of the outermost vacuum resonant component to the first off-resonant component) against  $\delta_U$ , while b) and c) plot the same ratio for the second and third off-resonant components. To be consistent with the results of figure 10, we would expect the ratio  $b_{m=nq}^1/b_{m=nq+1}^1$  to decrease with  $\delta_U$ , and the ratios  $b_{m=nq}^1/b_{m=nq+2}^1$  and  $b_{m=nq}^1/b_{m=nq+3}^1$  to both increase with  $\delta_U$ . Instead, the plot shows that all three ratios decrease with  $\delta_U$ . The field applied to the datapoints in figure 11 contains a full poloidal spectrum rather than just a single  $m_{BC}$  as in figure 10, so it is likely that the spectrum within the plasma is determined primarily by  $\Delta m = 1$  coupling between directly adjacent poloidal harmonics. That is, coupling between  $b_{m=nq}^1$  and  $b_{m=nq+2}^1$  is driven by a chain of  $\Delta m = 1$  from  $b_{m=nq+2}^1$  to  $b_{m=nq+1}^1$  to  $b_{m=nq}^1$ , rather than  $\Delta m = 2$  coupling between  $b_{m=nq+2}^1$  and  $b_{m=nq}^1$ . Figure 10 shows that the toroidicity induced  $\Delta m = 1$  coupling decreases with  $\delta_U$ , causing secondary coupling to  $\Delta m = 2, 3$  components to be reduced in Figure 11b) and c). The reduction in toroidicity induced coupling with  $\delta_U$  dominates over the increase in elongation and triangularity induced coupling. From this we may deduce that the peeling response drive of the resonant components is weaker in high triangularity, rather than stronger as proposed at the start of this section. This result strongly contradicts the theory that increased increased triangularity induced PHC between the peeling response and resonant components is the cause of the triangularity requirement for suppression. It should be noted that this result does not preclude a strong resonant field being part of the suppression mechanism, it merely indicates that any resonant field present is not the result of increased PHC due to raised triangularity.

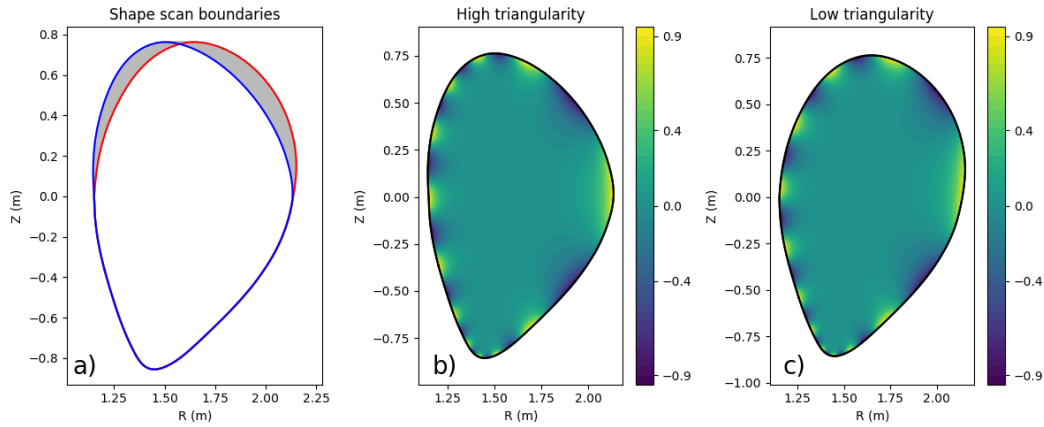


**Figure 9.** a) The boundary of a reference equilibrium reconstructed from discharge 30835 at 3.2s is distorted in order to scan the upper triangularity. The equilibrium is recomputed after boundary distortion using CHEASE to ensure self consistency. b,c) A single  $m$  vacuum magnetic perturbation,  $m_{BC} = 12$  in the above figure, is applied as a boundary condition at the plasma edge to each equilibrium in the shape scan.

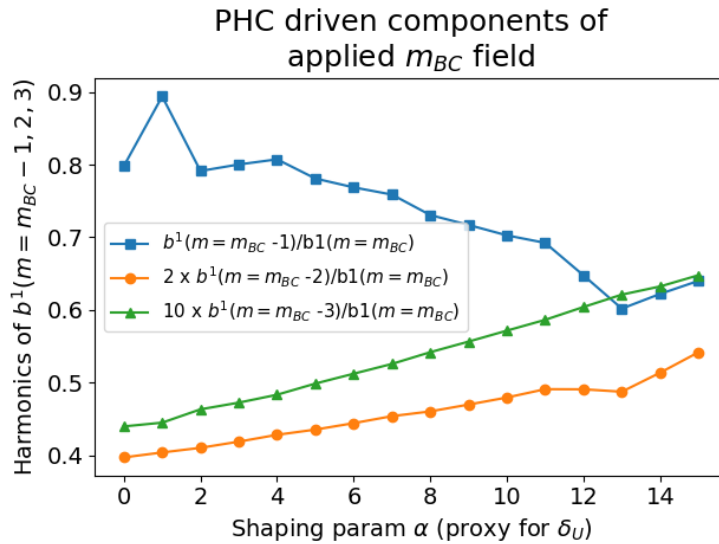


**Figure 10.** Harmonics with  $m$  below  $m_{BC}$ , at  $s = 0.997$ . These harmonics are not present in the applied field which is a pure  $m_{BC}$  field, and must be driven by PHC. Note that the  $m_{BC} - 2, 3$  lines have been rescaled for conciseness. The  $m_{BC} - 2, 3$  harmonics increase with  $\delta_U$ , while the  $m_{BC} - 1$  harmonic decreases. This indicates that elongation and triangularity induced PHC increase with  $\delta_U$ , while toroidicity induced PHC decreases.

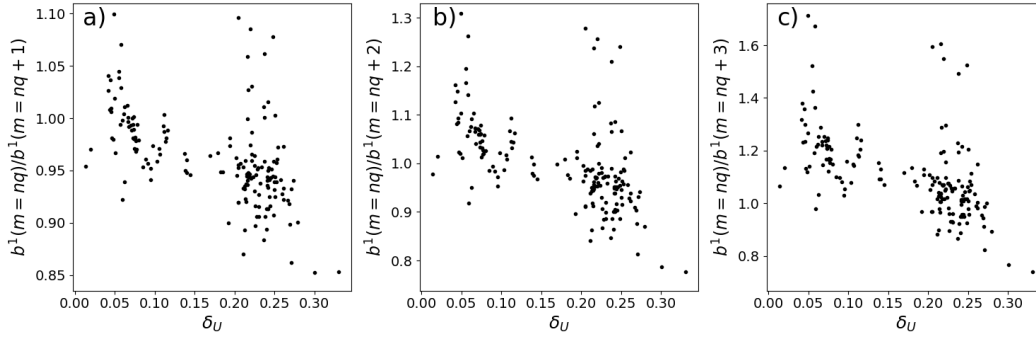


**Figure 11.** The outermost vacuum resonant component normalised to a) the first adjacent off-resonant component  $b_{m=nq+1}^1$  b) the second adjacent off-resonant component  $b_{m=nq+2}^1$  c) the third adjacent off-resonant component  $b_{m=nq+3}^1$ . These ratios indicate the extent of coupling between the resonant components and the adjacent off-resonant components, in the spectral region occupied by the peeling response. All three ratios decrease with  $\delta_U$ . This is interpreted as indicating that PHC between the resonant components and higher harmonics with  $\Delta m = 1, 2, 3$ , is dominated by toroidicity induced  $\Delta m = 1$  coupling which is seen in figure 10 to decrease with  $\delta_U$ .

## 5. Summary and Discussion

It is established experimentally on ASDEX Upgrade that ELM suppression access requires good coupling between the applied field and marginally stable edge MHD modes, here called the peeling response, as well as sufficiently high upper triangularity  $\delta_U$ [23]. Initially the requirement of high triangularity was explained by proposing that at high triangularity the P-B stability is enhanced, allowing the plasma to access higher pedestal pressure gradients which in turn boosts the peeling response, facilitating suppression access[2]. Considering the previously observed correlation[22] between peeling response induced plasma corrugation and density pump out, expecting a larger peeling response in the suppressed phase would also be consistent with the experimental observation of a sustained increase in the density pump out in the suppressed phase. In this work, a positive correlation between  $\delta_U$  and the pedestal pressure (consistent with previous work[25]), and a slight correlation between pedestal pressure and peeling response, are observed. However, the peeling response is actually found to be lower in general in the suppressed cases than the mitigated, rather than higher as the above theory leads us to expect. It is shown that a side effect of creating a high triangularity plasma on ASDEX Upgrade, is moving the plasma further from the ELM control coils, which causes the peeling response to decrease with plasma triangularity simply due to a lower effective vacuum field. The dependence of the peeling response on the pedestal pressure is weak, such that the effect of increasing the coil-plasma distance dominates over it. Therefore, the requirement of high  $\delta_U$  for suppression is not due to the requirement of an enhanced peeling response as previously supposed[2]. For fixed  $\delta_U$ , reduced pressure drive due to the enhanced density pump out of the suppressed phase further reduces the peeling response relative to the mitigated phase. The finding that the peeling response is

lower in the suppressed phase than mitigated, due to increased coil-plasma gap and lower density in the suppressed phase, also implies that the correlation between density pump out and edge corrugation does not hold for the suppression. This is consistent with experimental observations on the EAST tokamak[17]. The coil current was ramped linearly in time, and the density decreased due to RMP induced pump out. Once the suppression threshold was reached, the density suddenly dropped further, and then remained constant even as the coil current continued to increase, demonstrating that the correlation between the peeling response (which increases linearly with coil current) and density pump out had been broken. This suggests that the mechanism of the enhanced density pump out in the suppressed phase, is distinct from the mechanism for density pump out in the mitigated phase. This may be related to an observation on DIII-D, of an increase in long wavelength electron temperature turbulence during the RMP ELM suppressed phase relative to the RMP mitigated phase[36].

An alternative explanation for the high triangularity requirement is investigated. It is proposed here that increasing the triangularity would increase  $\Delta m = 3$  poloidal harmonic coupling, allowing the peeling response to more strongly drive the resonant components for fixed peeling response, facilitating field penetration. Applying a single harmonic boundary condition with harmonic number  $m_{BC}$  to a numerical scan of the upper triangularity, showed that the  $m = m_{BC} - 2, 3$  components, driven by elongation and triangularity induced coupling, increased with  $\delta_U$ . However the  $m_{BC} - 1$  component driven by toroidicity induced coupling decreased with  $\delta_U$ . To examine the effect of triangularity on poloidal harmonic coupling in realistic applied fields and plasma shapes, the ratio of the outermost resonant to the off resonant components computed for the assembled database, which includes wide variation in triangularity. If the hypothesis were correct, we would expect to see the ratio of  $b_{m=nq}^1/b_{m=nq+3}^1$  increase with triangularity. However, this ratio in fact decreases with triangularity, likely due to the dominance of toroidicity induced coupling (which decreases with  $\delta_U$ ) over triangularity induced coupling. The hypothesis that enhanced triangularity induced coupling may explain the high triangularity requirement of ELM suppression, is therefore rejected. The requirement may instead be due to a requirement of enhanced P-B stability to prevent interference of the mitigation mechanism, as discussed below.

It is shown previously that suppression access requires the applied field to be aligned to provide an amplified peeling response, and the density to be reduced below a certain threshold[23]. Plasma edge corrugation (driven by the peeling response) is correlated with density pump-out [22, 28], and is also implicated as a likely cause of mitigation, by reducing the P-B stability boundary of the resulting 3D deformed equilibria[10, 11, 12]. In particular, corrugation induced changes to the local geometry is predicted to cause a significant decrease in field line bending stabilisation for specific field lines[37], consistent with the observation of helically localised ballooning modes during RMP ELM mitigation on ASDEX Upgrade[12]. Correlations between the amplified peeling response and mitigated ELM frequency[28, 38] indicate increasing corrugation further degrades P-B stability. Therefore, as the peeling response increases (for example by a coil phase scan or current ramp), increasing density pump out is expected to move the pedestal operational point to more stable regions of  $(j, \alpha)$

space, but increasing corrugation also moves the P-B boundary following the operational point, as explained in [10]. With the coils off ELM crashes determine the pedestal limit, so we expect high and low  $\delta_U$  points to sit on their respective P-B boundaries, allowing high triangularity plasmas to achieve larger values of  $(j, \alpha)$ . However, with the RMP coils active, the resulting confinement degradation determines the pedestal limit, so the dependence of the pedestal gradient on  $\delta_U$  is significantly weakened, and we may expect the high and low  $\delta_U$  operational points to occupy similar regions of  $(j, \alpha)$  space. Figure 12b) and c) plot the points of the database in  $(j, \alpha)$  space, distinguishing between high and low  $\delta_U$  points and mitigation and suppression points respectively. It should be noted that the  $(j, \alpha)$  points in figure 12 are derived from equilibria produced by CLISTE, rather than by HELENA as is conventional for these plots[39]. However it has been shown that the edge current density of kinetically constrained CLISTE equilibria are in good agreement with predictions of neoclassical currents[40]. Points with significant PSL screening, coil misalignment or reduced coil current are excluded. The large overlap of the regions occupied by the high and low triangularity points in figure b) is consistent with our expectation that with coils active, the dependence of the pedestal gradient limit on  $\delta_U$  is weakened or broken. Using the ELITE code[41], finite-n peeling ballooning stability boundaries are computed for two representative high and low  $\delta_U$  points from the database, which demonstrate that the peeling-ballooning stability is significantly enhanced by increased shaping, consistent with previous predictions[25]. For the low  $\delta_U$  points, movement of the boundary with increasing corrugation is likely to overtake the operational point, keeping the operational point P-B unstable. This can be understood as suppression being precluded by the mitigation mechanism, and is consistent with a correlation between the peeling response and the reappearance of ELMs in suppressed phases reported in [42], and with the observation on JET that with  $n=1$  perturbations applied, ELMs may occur despite the plasma being predicted to be P-B stable[43]. Meanwhile the operational points for the high  $\delta_U$  cases are further from the P-B boundary and therefore more resilient to corrugation induced destabilisation. The above picture is sketched in Figure 12a), and may provide a basis for understanding the linear physics of the suppressed plasma state, and explaining why accessing suppression in low  $\delta_U$  is significantly more challenging than low  $\delta_U$ . The above theory implies the assumption that since unperturbed high  $\delta_U$  equilibria have greater stability than low  $\delta_U$  equilibria, then perturbed high  $\delta_U$  equilibria will have enhanced stability relative to perturbed low  $\delta_U$  equilibria. It is observed that the suppression transition is accompanied by an enhanced density pump out [23]. This work finds that in contrast to the mitigated phase, the enhanced pump out in suppression has no accompanying increase in the peeling response, and therefore no corresponding increasing in edge corrugation. Rather, enhanced pump out in the suppressed phase reduces the pressure drive for the peeling response, reducing the the edge corrugation. Therefore after the suppression transition, the operational point is expected to move further into the P-B stable region, while the stable region is expanded by the reduction in corrugation induced P-B destabilisation, increasing the gap between the operational point and P-B boundary. This effect may partially explain the observation that the conditions for maintaining suppression are less stringent than for entering it[23]. To test this theory, models must be developed

capable of mapping the P-B linear stability space of highly shaped experimental 3D equilibria including rotation, and the stability maps of high and low  $\delta_U$  3D equilibria, and suppressed and mitigated equilibria, compared. Several such models have been developed[44], or are near completion[45, 46, 47].

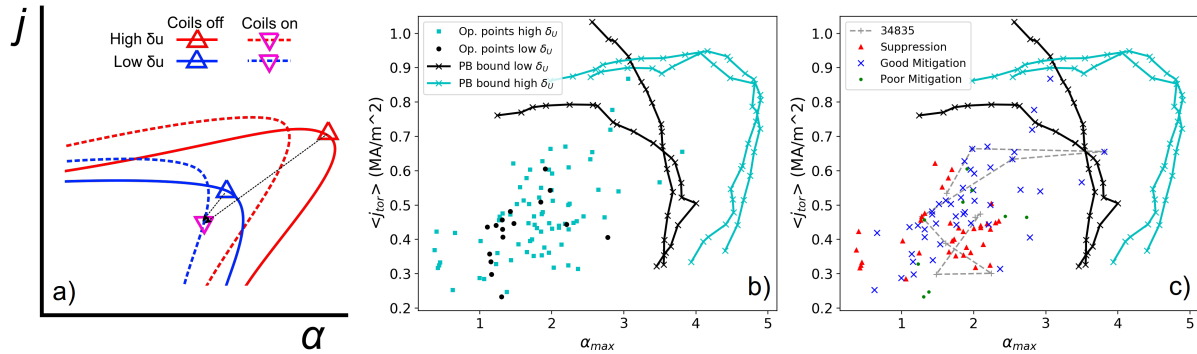


**Figure 12.** Sketch of the suggested picture of the high triangularity requirement, presented as an alternative explanation to the hypothesis in [2]. a) With increasing peeling response, density pump out moves the experimental point towards stability, while corrugation moves the stability boundary. This theory builds on the picture presented in figure 12 of [10], which explains how 3D corrugation induced movement of the P-B stability boundary relative to the operational point in ELM control experiments may lead either to mitigation or suppression. In low triangularity, it is suggested here that the boundary moves such that the experimental point remains always in the unstable region, whereas in high triangularity, the modified shape of the stability boundary allows the experimental point to enter the stable region for some values of the peeling response. b) The operational points in  $(j, \alpha)$  space for the database assembled in this work are plotted for high and low triangularity, along with P-B stability boundaries computed for two representative high and low  $\delta_U$  points in the database. The approximate co-location of the high and low  $\delta_U$  points suggests that the dependence of  $(j, \alpha)$  on  $\delta_U$  is weakened or broken by RMP induced confinement degradation. The distance from the operational points to the stability boundaries is therefore larger in the high  $\delta_U$  case, making these points more resilient to movement of the boundary by corrugation. c) The operational points in  $(j, \alpha)$  space for the database assembled in this work, excluding points for which the applied field is weak or misaligned, are plotted for suppression and mitigation points. In the suppressed, high triangularity cases, the enhanced density pump out observed in the suppressed phase appears to move the operational points still further into the stable region, with no corresponding movement of the stability boundary. This is consistent with the observation that the conditions to maintain suppression are less stringent than for suppression access.

Recent works indicate that the transition to suppression is a non-linear bifurcation process, involving a rapid penetration of the resonant field and the formation of one or more magnetic islands[17, 48]. With only linear physics as in the above picture, the suppression transition itself cannot be understood. By focussing on only established and slowly varying suppressed or mitigated phases as in this study, the problem of treating the non-linear transition is bypassed, and the suppressed state may be studied with only linear models. Furthermore, the single fluid model used in this study is unsuitable to describe the screening physics accurately, and therefore may not distinguish between the penetrated state which features islands, and the screened state. This study therefore focusses on the amplified peeling

response rather than the resonant response. It is not considered necessary to know the resonant response accurately to compute the peeling response, since although there is evidence that the peeling response can drive the resonant components[21, 49], there is currently no evidence of a causal relation in the opposite direction. This is consistent with agreement between resistive and ideal MHD codes (MARS-F and VMEC) on predictions of the peeling response[31]. The destabilisation due to 3D effects is driven by plasma surface corrugation, which is driven by the peeling response rather than the resonant response[10], so it is not expected that a penetrated plasma would have significantly different stability properties to an otherwise identical screened plasma. A strong resonant response would of course modify the rotation braking and edge transport properties, but the effects of these modifications manifest in the rotation and kinetic profiles, which can be measured and used as input to a linear model. Therefore a linear stability code which includes physics effects relevant to the P-B stability boundary (most notably, 3D corrugation and rotation) should be able to predict the stability of a suppressed penetrated plasma state even without knowledge of the bifurcation process by which it arrived at that state. Therefore the non-linear transition process described in [48] does not preclude the suppressed state being understood using linear response and stability models as proposed above.

## Acknowledgements

This work has been carried out within the framework of the EUROfusion Consortium and has received funding from the Euratom research and training programme 2014-2018 and 2019-2020 under grant agreement No 633053, and part-funded by the RCUK Energy Programme (under grant EP/P012450/1). To obtain further information on the data and models underlying this paper please contact PublicationsManager@ukaea.uk. The views and opinions expressed herein do not necessarily reflect those of the European Commission.

## References

- [1] H Meyer *et al*, 2017, *Nuclear Fusion*, **57**, 102014.
- [2] R Nazikian *et al*. First Observation of ELM Suppression by Magnetic Perturbations in ASDEX Upgrade and Comparison to DIII-D Matched-Shape Plasmas. In *26th IAEA Int. Conf. on Fusion Energy*, 1–8, Kyoto, Japan, 2016.
- [3] N Oyama, 2008, *Journal of Physics: Conference Series*, **123**, 012002.
- [4] A Loarte *et al*, 2003, *Plasma Physics and Controlled Fusion*, **45**, 1549–1569.
- [5] T E Evans *et al*, 2004, *Physical Review Letters*, **92**, 235003.
- [6] A Kirk *et al*, 2013, *Plasma Physics and Controlled Fusion*, **55**, 124003.
- [7] W Suttrop *et al*, 2011, *Physical Review Letters*, **106**, 225004.
- [8] I T Chapman *et al*, 2014, *Nuclear Fusion*, **54**, 083006.
- [9] A Kirk *et al*, 2012, *Physical Review Letters*, **108**, 255003.
- [10] I T Chapman *et al*, 2013, *Physics of Plasmas*, **20**, 056101.
- [11] C J Ham *et al*, 2014, *Physics of Plasmas*, **21**, 102501.
- [12] M Willensdorfer *et al*, 2017, *Physical Review Letters*, **119**, 085002.
- [13] A Kirk *et al*, 2013, *Nuclear Fusion*, **53**, 043007.
- [14] P R Thomas, 2008, *Proc. 22nd Int. Conf. on Fusion Energy 2008*.
- [15] W Suttrop *et al*, 2018, *Nuclear Fusion*, **58**, 096031.
- [16] Y M Jeon *et al*, 2012, *Physical Review Letters*, **109**, 035004.
- [17] Y Sun *et al*, 2016, *Physical Review Letters*, **117**, 115001.
- [18] Y Liu *et al*, 2010, *Physics of Plasmas*, **17**, 122502.
- [19] M J Lanctot *et al*, 2013, *Nuclear Fusion*, **53**, 083019.
- [20] S R Haskey *et al*, 2014, *Plasma Physics and Controlled Fusion*, **56**, 035005.
- [21] D A Ryan *et al*, 2015, *Plasma Physics and Controlled Fusion*, **57**, 095008.
- [22] Y Liu *et al*, 2011, *Nuclear Fusion*, **51**, 083002.
- [23] W Suttrop *et al*, 2017, *Plasma Physics and Controlled Fusion*, **59**, 014049.
- [24] R J Groebner *et al*, 1998, *Plasma Physics and Controlled Fusion*, **40**, 673–677.
- [25] F M Laggner *et al*, 2018, *Nuclear Fusion*, **58**, 046008.
- [26] P J Mc Carthy, 2012, *Plasma Physics and Controlled Fusion*, **54**, 015010.
- [27] W Suttrop *et al*. Physical description of external circuitry for Resistive Wall Mode control in ASDEX Upgrade. In *36th EPS Conference on Plasma Physics*, volume 33 E1, 458–461, 2009.
- [28] D A Ryan *et al*, 2018, *Plasma Physics and Controlled Fusion*, **60**, 065005.
- [29] J D King *et al*, 2015, *Physics of Plasmas*, **22**, 072501.
- [30] P Piovesan *et al*, 2017, *Plasma Physics and Controlled Fusion*, **59**, 014027.
- [31] M Willensdorfer *et al*, 2016, *Plasma Physics and Controlled Fusion*, **58**, 114004.
- [32] Y Liu *et al*, 2000, *Physics of Plasmas*, **7**, 3681.
- [33] D A Ryan *et al*, 2017, *Plasma Physics and Controlled Fusion*, **59**, 024005.
- [34] L Li *et al*, 2017, *Plasma Physics and Controlled Fusion*, **59**, 044005.
- [35] Y Liu *et al*, 2016, *Nuclear Fusion*, **56**, 056015.
- [36] C. Sung *et al*, 2017, *Physics of Plasmas*, **24**, 112305.
- [37] T B Cote *et al*, 2019, *Nuclear Fusion*, **59**, 016015.

- [38] A Kirk *et al*, 2015, *Nuclear Fusion*, **55**, 043011.
- [39] S Saarelma *et al*, 2013, *Nuclear Fusion*, **53**, 123012.
- [40] M G Dunne *et al*, 2012, *Nuclear Fusion*, **52**, 123014.
- [41] H R Wilson *et al*, 2002, *Physics of Plasmas*, **9**, 1277–1286.
- [42] A Wingen *et al*, 2015, *Plasma Physics and Controlled Fusion*, **57**, 104006.
- [43] S Saarelma *et al*, 2011, *Plasma Physics and Controlled Fusion*, **53**, 085009.
- [44] T Weyens *et al*, 2017, *Journal of Computational Physics*, **330**, 997–1009.
- [45] M S Anastopoulos-Tzani *et al*. Perturbative 3D Ideal MHD Stability of Tokamak Plasmas. In *45th EPS Conference on Plasma Physics*, 1–4, Prague, 2018.
- [46] E Strumberger *et al*, 2017, *Nuclear Fusion*, **57**, 016032.
- [47] C Nührenberg, 2016, *Nuclear Fusion*, **56**, 076010.
- [48] R Nazikian *et al*, 2015, *Physical Review Letters*, **114**, 105002.
- [49] F Orain *et al*, 2017, *Nuclear Fusion*, **57**, 022013.